Picosecond vs Femtosecond: Are All Laser Desorption Ionizations Created Equal?

Gabriel A. Stewart, Duke Debrah, Yasashri Ranathunga, Temitayo A. Olowolafe, H. Bernhard Schlegel, Suk Kyoung Lee, and Wen Li*

Read Online

ACCESS | Metrics & More | Article Recommendations

ABSTRACT: With a three-dimensional (3D) momentum imaging technique, we investigated the laser desorption ionization dynamics initiated by both chirped picosecond and femtosecond pulses. 3D momentum images of desorbed ions from 2,5-dihydroxybenzoic acid (DHB), a common laser desorption matrix, were obtained for the first time. A striking difference was observed between the processes initiated by femtosecond and picosecond pulses. The lack of initial momentum in ions produced by femtosecond pulses suggests a suppression of plume formation, which can be exploited to increase the sensitivity of matrix-assisted laser desorption ionization.
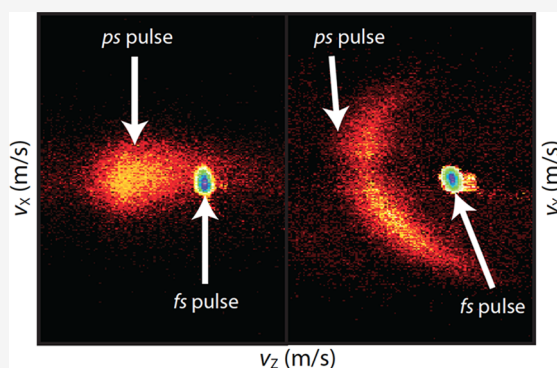
INTRODUCTION

Matrix-assisted laser desorption ionization (MALDI) is a powerful mass spectrometric method used for the mass analysis of nonvolatile mixtures and, more importantly, complex biomolecular compounds/samples.[1−3] Over the past three decades, there has been a significant focus on the development of the technique to increase the mass resolution and sensitivity for analyte detection. Generally, MALDI is performed by cocrystallization of the matrix-analyte solution on a substrate, which is then irradiated by resonant nanosecond ultraviolet (UV) laser pulses. Molecules/ions are ejected into the gas phase via plume formation, which contains mainly neutral species with minor ions (both cationic and anionic). The collisions in the plume facilitate proton transfer from the matrix ion to the analyte, which leads to analyte ionization. The analyte ion is then carried toward the detector for mass analysis. Although the technique is widely adopted, the origin of initial ion formation is still under debate. Various models such as thermal ionization,[4] energy pooling model,[5,6] thermal proton transfer,[7] jet expansion,[8] coupled chemical and physical dynamics (CCPD),[9] cluster ionization,[10] and photo-ionization and photochemical model[11] have been proposed but have not yet converged to a unified model.

Kinetic measurements after laser desorption/ionization have been of significant interest to help extract details about the initial ionization mechanism. Specifically, initial velocities of matrices and analytes have been justified as a significant marker for discriminating between MALDI mechanisms during desorption.[12−14] So far, a complete three-dimensional (3D)

characterization of the desorbed ions has not been achieved. Furthermore, even though a conventional MALDI experiment employs nanosecond lasers to initiate the desorption/ionization process, quite a few reports have shown that femtosecond pulses can achieve desorption/ionization.[15−23] Considering the large time scale difference between the two types of lasers and the typical dynamical time of electrons and lattices, we should expect the two processes to differ significantly. But in what way? A previous study employing nonresonant 800 nm excitation observed no difference between femtosecond and nanosecond pulse excitations.[23] Whether and how the dynamics differ after resonant excitation such as in MALDI has not been explored.

Utilizing imaging techniques to measure the momentum distributions of photoinduced fragments provides crucial information to the ionization/dissociation dynamics of atomic/molecular systems in gas phase[24,25] or from surfaces.[26−28] However, all of these systems measure the two-dimensional (2D) momenta of fragments. Recently, Li and co-workers have developed a 3D momentum imaging system to probe the surface decay dynamics of hot carriers in graphene.[29] The 3D momentum distributions of electrons emitted from the
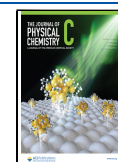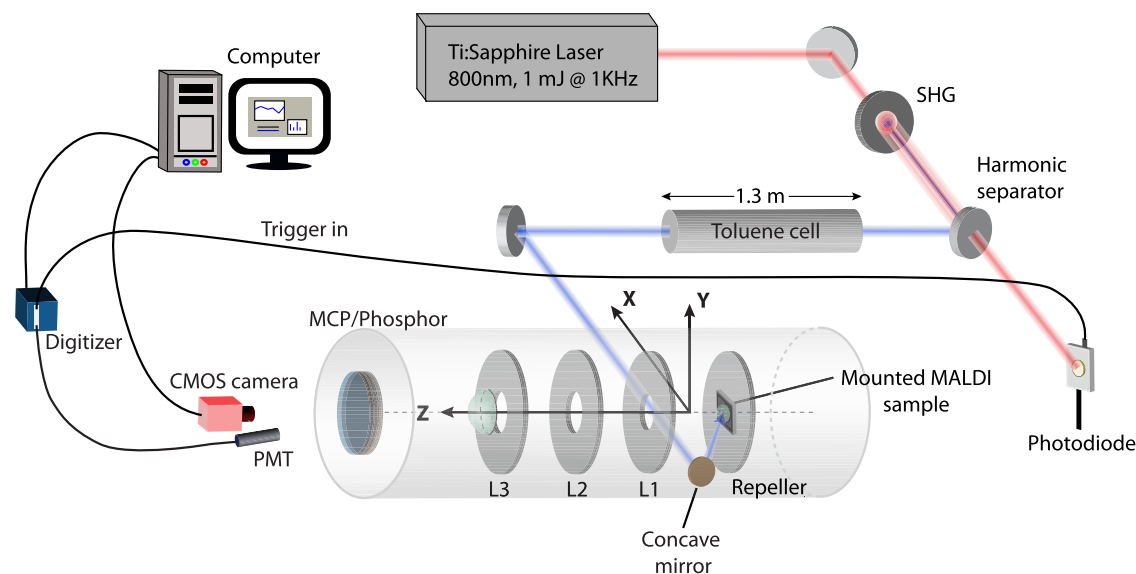
Figure 1. Schematic of the experimental setup for 3D momentum imaging of laser desorption/ionization.
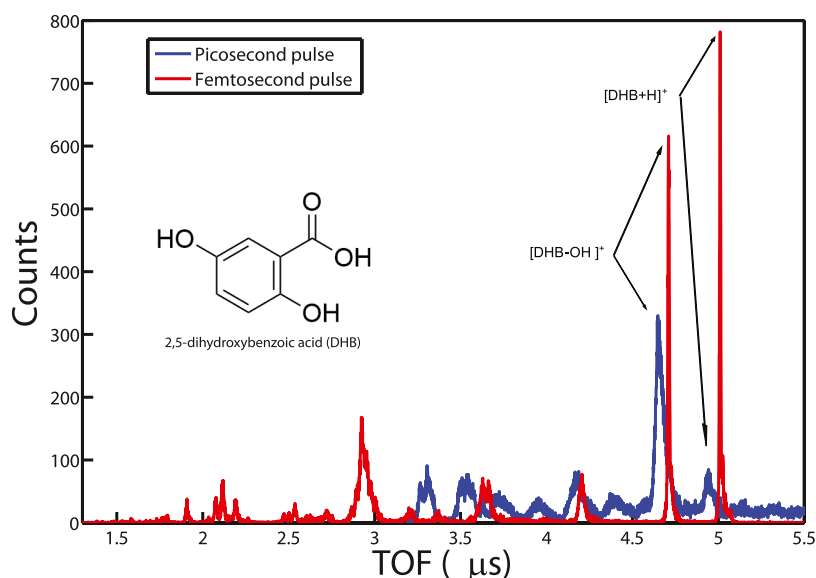

Figure 2. TOF spectra from SFI (femtosecond pulses) and LDI (picosecond pulses) of DHB. The inset shows the molecular structure of 2,5-DHB.

surface provided evidence of delayed photoemission. Conceptually, the same technique can be applied to study the laser desorption/ionization process by measuring the 3D momentum distributions of desorbed ions. Here in this work, we combined the technique with picosecond and femtosecond laser pulses and measured the 3D momentum images of ions with both lasers. Drastically different dynamics initiated by laser pulses with different pulse durations were revealed.

METHODS

The details of the setup have been described in previous experiments.[29−33] Here, we briefly describe modifications to the original instrumentation. For sample preparation, 2,5-Dihydroxybenzoic Acid (98%, Sigma-Aldrich) was prepared in a solution of 50:50 water/acetonitrile. The final concentration of the solution was 0.2 M, and several 2 μL spots were pipetted onto an indium tin oxide (ITO)-coated glass slide. The justification for using the conductive coating on the glass is to reduce charge buildup on the surface and to provide a constant

electric field for momentum imaging. The spots were left to crystallize in ambient conditions, and another application was performed to carefully fill the empty spaces between the neat 2,5-DHB crystals. The glass holder was placed on a stainless steel ring and mounted to an electrode within the vacuum chamber of a home-built VMI apparatus perpendicular to time-of-flight (TOF) axis. A 1 kHz Ti:Sapphire femtosecond laser system (800 nm, 30 fs, KMLabs, Red dragon) coupled with a second harmonic generation (SHG) crystal (BBO, 100 μm thick, United Crystal) to produce 400 nm light was used to ionize/desorb 2,5-DHB. A reflective geometric approach from a concave aluminum-coated mirror (f = 100 mm) was employed to desorb ions from the substrate at an angle of ∼45°. The size of the beam focal spot is estimated to be about 200 μm (x direction) ×50 μm (y direction) with an oval shape due to the focusing geometry and off-axis aberration. The schematic of the experimental setup is shown in Figure 1.

Two irradiation methods were employed for this experiment. We term strong-field ionization (SFI) as the approach
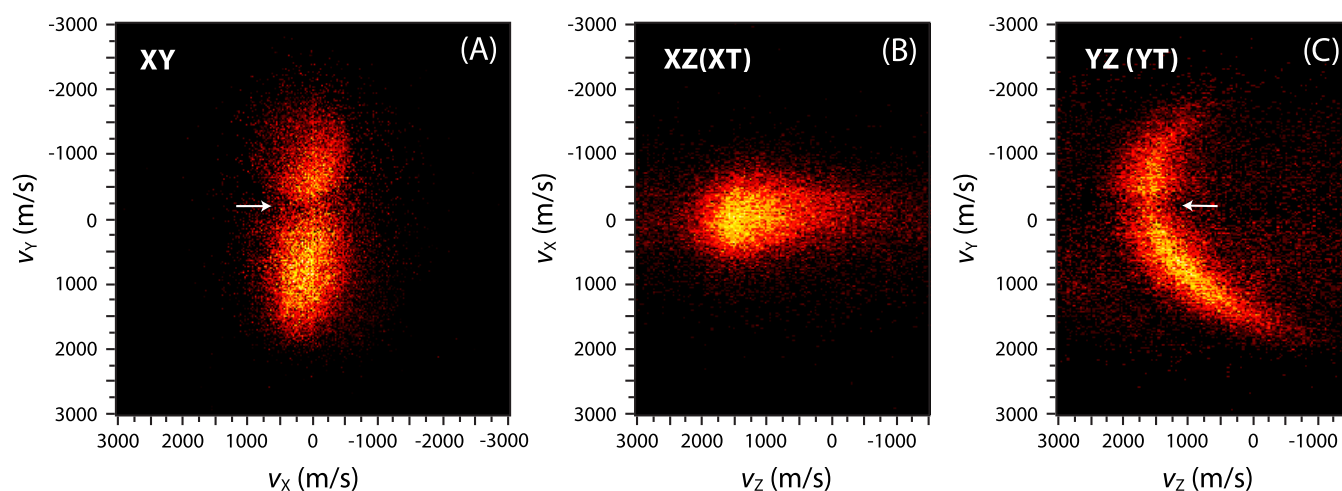
Figure 3. 3D velocity distributions of dehydroxylated DHB ion ([DHB−OH]$^+$) (137 Da) produced by picosecond pulses. $T(z)$ is the TOF axis, and X and Y are the spatial coordinates. The small discontinuities in panel (A) and (C) indicated by the arrows are not physical. They are due to defects in the imaging detector.

when applying femtosecond (fs) pulses to the sample at intensities of $\sim 10^{12}$ W/cm^2. The alternative method of ionization is laser desorption (LDI), where picosecond (ps) pulses at intensities of $<10^8$ W/cm^2 were employed. To produce the needed picosecond pulses, a long toluene cell (1.3 m in length) was used to stretch the femtosecond pulse (~ 40 fs) to picosecond pulse duration (~ 40 ps) by adding group delay dispersion (GDD) of 4.8 ps^2. Toluene was selected because it has low absorption at 400 nm and has a high group velocity dispersion (GVD) value (373 fs^2/mm).[34] This approach rules out spectrum variation, normally associated with different pulse durations, as one of the reasons for the observed different dynamics. We note the pulse was significantly chirped. Two harmonic separators were used to filter the fundamental laser at 800 nm. A dual MCP/phosphor (Photonis) was used to detect photoionized events. A complementary metal−oxide−semiconductor (CMOS) camera (Basler acA640-750 μm) triggered by a photodiode was used to capture images on the MCP/phosphor to provide spatial x and y coordinates. A high-speed digitizer (National Instruments, PXI 5162) with a sampling rate of 1.25 GS/s was coupled with a photomultiplier tube (PMT) (Hamamatsu, R928) to acquire the full waveform signal of ion events arriving at the detector. A peak detection algorithm was applied to each digitizer trace to extract the TOF of each ion. 3D momentum imaging is achieved by correlating the acquired TOF values from the digitizer and spatial coordinates provided by the camera and MCP/phosphor screen for each event. To reduce background signal such as Na$^+$ and K$^+$, the high voltage applied to MCP detector was pulsed to only turn on the detector during a selected TOF range. For 3D momentum measurements, the count rates must maintain at a few counts/pulse. If there is more than one event in a laser pulse, the brightness of the ion spots on the camera and the peak height of the TOF peaks will be used to correlate the hit positions and TOFs.[30] A TOF resolution of about 1 ns was achieved.

■ RESULTS AND DISCUSSION

The measured TOF spectra for both pulses are shown in Figure 2. In SFI and LDI, both dehydroxylated DHB ion ([DHB−OH]$^+$) (137 Da) and protonated DHB ion ([DHB+H]$^+$) (155 Da) are clearly visible, suggesting successful laser

desorption and ionization in both cases. However, the relative abundances are different. For SFI, we observed the dominant peak to be protonated DHB ion ([DHB+H]$^+$), while for LDI, the dehydroxylated DHB ion ([DHB−OH]$^+$) is more prominent. A subtle shift in the TOF spectra of approximately 0.1 μs is noted between SFI and LDI, which seems surprising. But we will return to this observation later in more detail. It is also clear that the peak widths are significantly different, which suggests a difference in initial velocity. In comparison with a spectrum of standard MALDI spectrum of DHB (see for example, ref 35, 36), the relative abundance between protonated DHB ion ([DHB+H]$^+$) and dehydroxylated DHB ion ([DHB−OH]$^+$) in LDI is a much closer match than that of SFI. This suggests that picosecond lasers are likely to initiate laser desorption ionization via a process that is similar to that of nanosecond laser pulses, while femtosecond pulses differ significantly.

With the coincidence measurement between the TOF and the hit position on the detector of each individual ion, the 3D momentum distributions were constructed. Figure 3 shows the momentum distributions of the LDI process together with its overall TOF. To calculate the velocity distributions, we used the following equation to convert TOFs to velocities along the TOF axis: $V_t = a\Delta t$, in which V_t is the initial velocity along the TOF axis and a is the acceleration of the ion in an electric field given by $a = \frac{qE}{m}$. E is the electric field potential that the ion is experiencing from the ion lenses, which was determined using SIMION, q is the charge of the particle, and m is the mass of the ion. Δt is the relative difference between the TOF of each ion's hit and that of SFI. Here, we used the sharp TOF peak of SFI event as the velocity zero reference for the two masses. This is corroborated by two facts. (1) the size of the images of SFI are small, suggesting vanishing velocity in the x, y direction. This is unlikely if a significant velocity is present along the TOF axis, considering the extensive collision process before the desorption. (2) the relative TOF difference between [DHB+H]$^+$ and [DHB−OH]$^+$ was perfectly matched, assuming a zero initial velocity for both masses (mass 137:155 vs TOFs 4.72 μs: 5.02 μs). The velocity perpendicular to the TOF axis (V_x, V_y) was calculated by $R_x R_y/TOF$, with Rx and Ry being the distance from the center of the images on the
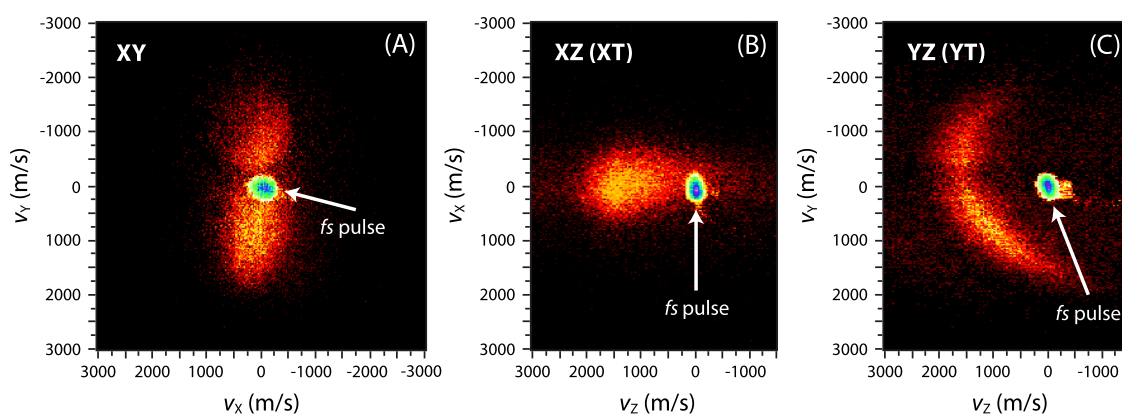
Figure 4. Comparison of the 3D velocity distributions of dehydroxylated DHB ion ([DHB−OH]⁺) produced by laser desorption/ionization driven by long picosecond pulses (∼40 ps) and femtosecond pulses (∼40 fs). The diffusive features are from picosecond pulses (same as in Figure 3), suggesting significant initial momenta of ions, while the small dot-like features are from femtosecond pulse excitation and are with near-zero momenta.

detector and TOF the time of flight of each event. The obtained initial velocities along the TOF axis for [DHB+H]⁺ and [DHB−OH]⁺ were around 1600 ± 200 and 1700 ± 200 m/s, respectively. These are in good agreement with those in previous MALDI measurement using nanosecond pulses.[37,38] The velocity is also quite directional, mainly pointing away from the surface. The high initial velocity and narrow angular distribution confirm the presence of plume formation. A surprising observation is the asymmetric momentum distributions in the plane parallel to the surface (plane *XY*): one direction (*Y*) has a larger velocity distribution than the other (*X*) (Figure 3A). This could not be observed in previous 1D or 2D momentum measurement of MALDI.

Considering the oval shape of the focal spot of the laser on the surface, it might be tempting to draw a conclusion that the asymmetry is due to the spatial asymmetry of the focal spots. However, because the observed asymmetries are orthogonal to each other, *i.e.*, the laser ellipse is horizontal while the momentum ellipse is vertical (Figures 1 vs 3A), the likely cause for this is not a simple spatial imaging effect. The observation suggests that the plume formation in MALDI is subjected to an *aperture(slit) effect*: a small spatial extension leading to a broader momentum distribution.[39] This is interesting, and it also has practical implications because a broad momentum distribution of desorbed ions can be detrimental to achieving high mass resolution. Overall, the relative abundance and the initial velocity suggest the picosecond and nanosecond laser initiate similar laser desorption ionization processes in DHB. This validation is important because this will enable high-resolution time-resolved investigations of MALDI dynamics using picosecond lasers. Such a study is very difficult with nanosecond lasers.

Now we move to discuss the 3D momentum distributions of SFI-initiated ions, as shown in Figure 4. For comparison, we plot the momentum distributions of both processes together. It shows drastically different momentum distributions: the initial velocities in all three dimensions approach zero for SFI. It has become clear on the reason for the TOF shift noted earlier: the nearly zero initial velocity arising from femtosecond pulse excitation does not change the TOF significantly contrary to the significant initial velocity of LDI, which reduces the TOF. The peak width's difference is also a result of different momentum distributions.

The difference in the 3D momentum distributions between LDI and SFI reveals different underlying dynamics of laser desorption ionization driven by femtosecond and picosecond pulses. The vanishing momenta in the SFI process indicate the absence of plume formation, which is contrary to LDI or conventional MALDI. This result, however, is not entirely surprising. The plume formation requires extensive heating of the crystal lattice and injection of energy into the nuclear degrees of freedom. This can be efficiently achieved by lasers with a pulse duration comparable to or longer than the electron−phonon coupling time, which is typically a few picoseconds. For femtosecond pulse excitation, the two-temperature model[40,41] is more appropriate for describing the dynamics due to the decoupling between the electronic and lattice dynamics. In this model, femtosecond pulses first excite electronic degrees of freedom of the system and increase the electron temperature significantly. This is somewhat self-limiting because ionization through thermionic emission will take place if a very high electron temperature is reached, and the system can lose energy. After the initial laser excitation, the electronic temperature will decrease and the lattice temperature will increase due to electron−phonon coupling, eventually equalizing. However, the rise of lattice temperature is much smaller due to a large heat capacity difference between the electron and lattice. This would suggest a large internal energy difference in the lattice between SFI and LDI. The relative abundance between dehydroxylated DHB ion ([DHB−OH]⁺) (137 Da) and protonated DHB ion ([DHB+H]⁺) (155 Da) offers clear evidence for this (Figure 2). In LDI, the fragment ion ([DHB−OH]⁺) has a much higher yield than that of the parent DHB ions, which suggests a higher internal temperature in DHB ions. Conversely, in SFI, the parent DHB ion has a higher yield. This is also consistent with the fact that the dehydration reaction is endothermic (ΔG^0 was calculated to be 24.7 kcal/mol at the B3LYP/6-31G(d, p) level).

If SFI does not produce a plume, how are ions ejected from the surface, as observed in our experiment? Because of the short pulse duration and, thus, a high laser intensity, direct multiphoton ionization is important, especially due to the presence of resonance excitation.[42] It is possible that due to significant ionization by the short pulse and prompt departure of ionized electrons, a small area on the surface is positively charged after laser irradiation and Coulombic repulsion can

desorb ions from the surface, similar to Coulombic explosion in multiply charged molecules. However, because the distance between neighboring molecules is typically large in molecular crystals such as DHB, the Coulombic repulsion will barely desorb the molecules from the surface without imparting much kinetic energy. This proposed mechanism is different from the well-established DIET (desorption induced by electronic transitions)[43,44] mechanism. Here, multiple ionization instead of electronic excitations initiates the desorption process. Furthermore, in DIET, desorbed neutral and ions typically have high kinetic energies (1 eV or higher), which is not the case here.

It should be noted that even though our current study with SFI suggests no plume formation, it does not mean femtosecond pulses cannot produce a plume in general. Previous laser ablation experiments with pulse durations as short as 5 *fs* have observed extensive material loss, albeit at much higher laser intensities and a different laser wavelength.[45] Due to the high sensitivity of our measurement (single ion detection), our study operates at a laser intensity of 2−3 orders lower than in previous femtosecond laser ablation experiments. Our results suggest laser intensity plays an important role in dictating the desorption dynamics using femtosecond pulses.

CONCLUSIONS

To summarize, 3D momentum images of desorbed ions from 2,5-dihydroxybenzoic acid (DHB), a common laser desorption matrix, were obtained for the first time with both femtosecond and chirped picosecond pulses. Clear evidence suggests picosecond pulses initiate MALDI-like processes driven by nanosecond pulses. This will allow future time-resolved studies on MALDI to utilize picosecond pulses to improve the achievable time resolution. Furthermore, it was found that the plume formation in MALDI, especially the momentum distributions, are modulated by the shape of the laser spots. Laser desorption initiated by femtosecond pulses is quite unique in that it avoids violent plume formation, and this can be exploited to prevent extensive loss of neutral molecules, thus increasing the sensitivity of the process. In the future, it will be interesting to study how SFI works with analytes cocrystallized with matrices such as DHB.

AUTHOR INFORMATION

Corresponding Author

    Wen Li − *Department of Chemistry, Wayne State University, Detroit, Michigan 48202, United States;* ⊙ orcid.org/0000-0002-3721-4008; Email: wli@chem.wayne.edu

Authors

    Gabriel A. Stewart − *Department of Chemistry, Wayne State University, Detroit, Michigan 48202, United States*

    Duke Debrah − *Department of Chemistry, Wayne State University, Detroit, Michigan 48202, United States;* ⊙ orcid.org/0000-0002-1281-3012

    Yasashri Ranathunga − *Department of Chemistry, Wayne State University, Detroit, Michigan 48202, United States*

    Temitayo A. Olowolafe − *Department of Chemistry, Wayne State University, Detroit, Michigan 48202, United States;* ⊙ orcid.org/0000-0003-2334-2997

    H. Bernhard Schlegel − *Department of Chemistry, Wayne State University, Detroit, Michigan 48202, United States;* ⊙ orcid.org/0000-0001-7114-2821

    Suk Kyoung Lee − *Department of Chemistry, Wayne State University, Detroit, Michigan 48202, United States*

Complete contact information is available at:
https://pubs.acs.org/10.1021/acs.jpcc.2c06573

Notes

The authors declare no competing financial interest.

REFERENCES

(1) Beaufour, M.; Ginguené, D.; Le Meur, R.; Castaing, B.; Cadene, M. Liquid Native Maldi Mass Spectrometry for the Detection of Protein-Protein Complexes. *J. Am. Soc. Mass Spectrom.* **2018**, *29*, 1981.

(2) Han, X.; Aslanian, A.; Yates, J. R., 3rd. Mass Spectrometry for Proteomics. *Curr. Opin. Chem. Biol.* **2008**, *12*, 483.

(3) Edwards, J. R.; Ruparel, H.; Ju, J. Mass-Spectrometry DNA Sequencing. *Mutat. Res., Fundam. Mol. Mech. Mutagen.* **2005**, *573*, 3.

(4) Bae, Y. J.; Kim, M. S. A Thermal Mechanism of Ion Formation in Maldi. *Annu. Rev. Anal. Chem.* **2015**, *8*, 41.

(5) Zenobi, R.; Knochenmuss, R. Ion Formation in Maldi Mass Spectrometry. *Mass Spectrom. Rev.* **1999**, *17*, 337.

(6) Knochenmuss, R. Ion Formation Mechanisms in UV-Maldi. *Analyst* **2006**, *131*, 966.

(7) Lu, I. C.; Lee, C.; Lee, Y.-T.; Ni, C.-K. Ionization Mechanism of Matrix-Assisted Laser Desorption/Ionization. *Annu. Rev. Anal. Chem.* **2015**, *8*, 21.

(8) Trimpin, S.; Inutan, E. D.; Herath, T. N.; McEwen, C. N. Laserspray Ionization, a New Atmospheric Pressure Maldi Method for Producing Highly Charged Gas-Phase Ions of Peptides and Proteins Directly from Solid Solutions. *Mol. Cell. Proteomics* **2010**, *9*, 362.

(9) Knochenmuss, R. The Coupled Chemical and Physical Dynamics Model of Maldi. *Annu. Rev. Anal. Chem.* **2016**, *9*, 365.

(10) Karas, M.; Krüger, R. Ion Formation in Maldi: The Cluster Ionization Mechanism. *Chem. Rev.* **2003**, *103*, 427.

(11) Ehring, H.; Karas, M.; Hillenkamp, F. Role of Photoionization and Photochemistry in Ionization Processes of Organic Molecules and Relevance for Matrix-Assisted Laser Desorption Lonization Mass Spectrometry. *Org. Mass Spectrom.* **1992**, *27*, 472.

(12) Juhasz, P.; Vestal, M. L.; Martin, S. A. On the Initial Velocity of Ions Generated by Matrix-Assisted Laser Desorption Ionization and Its Effect on the Calibration of Delayed Extraction Time-of-Flight Mass Spectra. *J. Am. Soc. Mass Spectrom.* **1997**, *8*, 209.

(13) Glückmann, M.; Karas, M. The Initial Ion Velocity and Its Dependence on Matrix, Analyte and Preparation Method in Ultraviolet Matrix-Assisted Laser Desorption/Ionization. *J. Mass Spectrom.* **1999**, *34*, 467.

(14) Karas, M.; Bahr, U.; Fournier, I.; Glückmann, M.; Pfenninger, A. The Initial-Ion Velocity as a Marker for Different Desorption-Ionization Mechanisms in Maldi. *Int. J. Mass Spectrom.* **2003**, *226*, 239.

(15) Wichmann, J.; Lupulescu, C.; Wöste, L.; Lindinger, A. Matrix Assisted Laser Desorption/Ionization of Potassium Adapted Angio-tensine Ii Using Femtosecond Laser Pulses. *Eur. Phys. J. D* **2009**, *52*, 151.

(16) Shirota, T.; Tsuge, M.; Hikosaka, Y.; Soejima, K.; Hoshina, K. Detection of Neutral Species in the Maldi Plume Using Femtosecond Laser Ionization: Quantitative Analysis of Maldi-Ms Signals Based on

a Semiequilibrium Proton Transfer Model. *J. Phys. Chem. A* **2017**, *121*, 31.

(17) Phan, T. D.; Li, A.; Nakamura, H.; Imasaka, T.; Imasaka, T. Single-Photon Ionization Mass Spectrometry Using a Vacuum Ultraviolet Femtosecond Laser. *J. Am. Soc. Mass Spectrom.* **2020**, *31*, 1730.

(18) Meffert, A.; Grotemeyer, J. Formation, Stability and Fragmentation of Biomolecular Clusters in a Supersonic Jet Investigated with Nano- and Femtosecond Laser Pulses. *Ber. Bunsenges. Phys. Chem.* **1998**, *102*, 459.

(19) Cui, Y.; Bhardwaj, C.; Milasinovic, S.; Carlson, R. P.; Gordon, R. J.; Hanley, L. Molecular Imaging and Depth Profiling of Biomaterials Interfaces by Femtosecond Laser Desorption Postionization Mass Spectrometry. *ACS Appl. Mater. Interfaces* **2013**, *5*, 9269.

(20) Chekalin, S. V.; Golovlev, V. V.; Kozlov, A. A.; Matveets, Y. A.; Yartsev, A. P.; Letokhov, V. S. Femtosecond Laser Photoionization Mass Spectrometry of Tryptophan-Containing Proteins. *J. Phys. Chem. A* **1988**, *92*, 6855.

(21) Wichmann, J. M.; Lupulescu, C.; Wöste, L.; Lindinger, A. Matrix-Assisted Laser Desorption/Ionization by Using Femtosecond Laser Pulses in the near-Infrared Wavelength Regime. *Rapid Commun. Mass Spectrom.* **2009**, *23*, 1105.

(22) Arnolds, H.; Rehbein, C. E. M.; Roberts, G.; Levis, R. J.; King, D. A. Femtosecond near-Infrared Laser Desorption of Multilayer Benzene on Pt{111}: Spatial Origin of Hyperthermal Desorption. *Chem. Phys. Lett.* **1999**, *314*, 389.

(23) Arnolds, H.; Rehbein, C.; Roberts, G.; Levis, R. J.; King, D. A. Femtosecond near-Infrared Laser Desorption of Multilayer Benzene on Pt{111}: A Molecular Newton's Cradle? *J. Phys. Chem. B* **2000**, *104*, 3375.

(24) Chandler, D. W.; Houston, P. L. Two-Dimensional Imaging of State-Selected Photodissociation Products Detected by Multiphoton Ionization. *J. Chem. Phys.* **1987**, *87*, 1445.

(25) Eppink, A. T. J. B.; Parker, D. H. Velocity Map Imaging of Ions and Electrons Using Electrostatic Lenses: Application in Photoelectron and Photofragment Ion Imaging of Molecular Oxygen. *Rev. Sci. Instrum.* **1997**, *68*, 3477.

(26) Czyzewski, J. J.; Madey, T. E.; Yates, J. T. Angular Distributions of Electron-Stimulated-Desorption Ions: Oxygen on W(100). *Phys. Rev. Lett.* **1974**, *32*, 777.

(27) Koehler, S. P. K.; Ji, Y.; Auerbach, D. J.; Wodtke, A. M. Three-Dimensional Velocity Map Imaging of Kbr Surface Photochemistry. *Phys. Chem. Chem. Phys.* **2009**, *11*, 7540.

(28) Tsai, M.-T.; Lee, S.; Lu, I. C.; Chu, K. Y.; Liang, C.-W.; Lee, C. H.; Lee, Y. T.; Ni, C.-K. Ion-to-Neutral Ratio of 2,5-Dihydroxybenzoic Acid in Matrix-Assisted Laser Desorption/Ionization. *Rapid Commun. Mass Spectrom.* **2013**, *27*, 955.

(29) Fan, L.; Lee, S. K.; Chen, P.-Y.; Li, W. Observation of Nanosecond Hot Carrier Decay in Graphene. *J. Phys. Chem. Lett.* **2018**, *9*, 1485.

(30) Lee, S. K.; Cudry, F.; Lin, Y. F.; Lingenfelter, S.; Winney, A. H.; Fan, L.; Li, W. Coincidence Ion Imaging with a Fast Frame Camera. *Rev. Sci. Instrum.* **2014**, *85*, No. 123303.

(31) Fan, L.; Lee, S. K.; Tu, Y. J.; et al. A New Electron-Ion Coincidence 3D Momentum-Imaging Method and Its Application in Probing Strong Field Dynamics of 2-Phenylethyl-N,N-Dimethylamine. *J. Chem. Phys.* **2017**, *147*, No. 013920.

(32) Lee, S. K.; Lin, Y. F.; Lingenfelter, S.; Fan, L.; Winney, A. H.; Li, W. Communication: Time- and Space-Sliced Velocity Map Electron Imaging. *J. Chem. Phys.* **2014**, *141*, No. 221101.

(33) Basnayake, G.; Ranathunga, Y.; Lee, S. K.; Li, W. Three-Dimensional (3D) Velocity Map Imaging: From Technique to Application. *J. Phys. B: At., Mol. Opt. Phys.* **2022**, *55*, No. 023001.

(34) Kozma, I. Z.; Krok, P.; Riedle, E. Direct Measurement of the Group-Velocity Mismatch and Derivation of the Refractive-Index Dispersion for a Variety of Solvents in the Ultraviolet. *J. Opt. Soc. Am. B* **2005**, *22*, 1479.

(35) Teearu, A.; Vahur, S.; Haljasorg, U.; Leito, I.; Haljasorg, T.; Toom, L. 2,5-Dihydroxybenzoic Acid Solution in Maldi-Ms: Ageing and Use for Mass Calibration. *J. Mass Spectrom.* **2014**, *49*, 970.

(36) Wallace, W. E.; Arnould, M. A.; Knochenmuss, R. 2,5-Dihydroxybenzoic Acid: Laser Desorption/Ionisation as a Function of Elevated Temperature. *Int. J. Mass Spectrom.* **2005**, *242*, 13.

(37) Bökelmann, V.; Spengler, B.; Kaufmann, R. Dynamical Parameters of Ion Ejection and Ion Formation in Matrix-Assisted Laser Desorption/Ionization. *Eur. J. Mass Spectrom.* **1995**, *1*, 81.

(38) Tomalová, I.; Frankevich, V.; Zenobi, R. On Initial Ion Velocities in Maldi: A Novel Ft-Icr Ms Approach. *Int. J. Mass Spectrom.* **2014**, *372*, 51.

(39) Kools, J. C. S.; Baller, T. S.; De Zwart, S. T.; Dieleman, J. Gas Flow Dynamics in Laser Ablation Deposition. *J. Appl. Phys.* **1992**, *71*, 4547.

(40) Fujimoto, J. G.; Liu, J. M.; Ippen, E. P.; Bloembergen, N. Femtosecond Laser Interaction with Metallic Tungsten and Non-equilibrium Electron and Lattice Temperatures. *Phys. Rev. Lett.* **1984**, *53*, 1837.

(41) Qiu, T. Q.; Tien, C. L. Short-Pulse Laser Heating on Metals. *Int. J. Heat Mass Transf.* **1992**, *35*, 719.

(42) Allwood, D. A.; Dreyfus, R. W.; Perera, I. K.; Dyer, P. E. UV Optical Absorption of Matrices Used for Matrix-Assisted Laser Desorption/Ionization. *Rapid Commun. Mass Spectrom.* **1996**, *10*, 1575.

(43) Avouris, P.; Walkup, R. E. Fundamental Mechanisms of Desorption and Fragmentation Induced by Electronic Transitions at Surfaces. *Annu. Rev. Phys. Chem.* **1989**, *40*, 173.

(44) Prybyla, J. A.; Heinz, T. F.; Misewich, J. A.; Loy, M. M. T.; Glownia, J. H. Desorption Induced by Femtosecond Laser Pulses. *Phys. Rev. Lett.* **1990**, *64*, 1537.

(45) Lenzner, M.; Krüger, J.; Sartania, S.; Cheng, Z.; Spielmann, C.; Mourou, G.; Kautek, W.; Krausz, F. Femtosecond Optical Breakdown in Dielectrics. *Phys. Rev. Lett.* **1998**, *80*, 4076.

▣ Recommended by ACS